ACS OMEGA

Article

Cite This: ACS Omega 2019, 4, 9850−9859

http://pubs.acs.org/journal/acsodf

Reactivity of Bioinspired Magnesium−Organic Networks under CO_2 and O_2 Exposure

Daniel E. Hurtado Salinas,[†,‡] Ane Sarasola,[§,∥] Bart Stel,[†,‡] Fernando P. Cometto,*[,†,‡,⊥] Klaus Kern,[‡,#] Andrés Arnau,[∥,∇,○] and Magalí Lingenfelder*[,†,‡]

[†]Max Planck-EPFL Laboratory for Molecular Nanoscience, EPFL SB CMNT NL-CMNT, CH 1015 Lausanne, Switzerland

[‡]Institut de Physique, École Polytechnique Fédérale de Lausanne, CH-1015 Lausanne, Switzerland

[§]Departamento de Física Aplicada I, UPV/EHU, Plaza Europa 1, E-20018 San Sebastián, Spain

[∥]Donostia International Physics Center (DIPC), Paseo Manuel de Lardizabal 4, E-20018 San Sebastián, Spain

[⊥]Departamento de Fisicoquímica, Instituto de Investigaciones en Fisicoquímica de Córdoba, INFIQC-CONICET, Facultad de Ciencias Químicas, Universidad Nacional de Córdoba, Ciudad Universitaria, X5000HUA Córdoba, Argentina

[#]Max-Planck-Institut für Festkörperforschung, D-70569 Stuttgart, Germany

[∇]Departamento de Física de Materiales, UPV/EHU, Paseo Manuel de Lardizabal 3, E-20018 San Sebastián, Spain

[○]Centro de Física de Materiales (CFM) CSIC-UPV/EHU, Materials Physics Center MPC, Paseo Manuel de Lardizabal 5, E-20018 San Sebastián, Spain

Supporting Information

ABSTRACT: Photosynthesis is the model system for energy conversion. It uses CO_2 as a starting reactant to convert solar energy into chemical energy, i.e., organic molecules or biomass. The first and rate-determining step of this cycle is the immobilization and activation of CO_2, catalyzed by RuBisCO enzyme, the most abundant protein on earth. Here, we propose a strategy to develop novel biomimetic two-dimensional (2D) nanostructures for CO_2 adsorption at room temperature by reductionist mimicking of the Mg−carboxylate RuBisCO active site. We present a method to synthesize a 2D surface-supported system based on Mg^{2+} centers stabilized by a carboxylate environment and track their structural dynamics and reactivity under either CO_2 or O_2 exposure at room temperature. The CO_2 molecules adsorb temporarily on the Mg^{2+} centers, producing a charge imbalance that catalyzes a phase transition into a different configuration, whereas O_2 adsorbs on the Mg^{2+} center, giving rise to a distortion in the metal−organic bonds that eventually leads to the collapse of the structure. The combination of bioinspired synthesis and surface reactivity studies demonstrated here for Mg-based 2D ionic networks holds promise for the development of new catalysts that can work at room temperature.

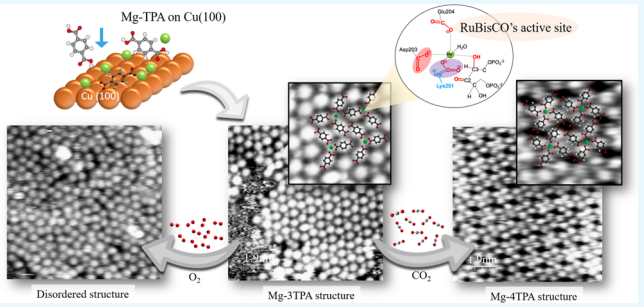

INTRODUCTION

For almost 3 billion years, nature has developed fantastic methods to convert solar energy to fuels in a way that humans are trying to replicate. This process is called photosynthesis,[1] which occurs in two steps: the light reactions (which require light) and carbon fixation (also known as the dark reaction or Calvin cycle). Up to now, there exists only a single conversion technology with prospects for long-term large-scale use: photovoltaics.[2,3] In a photovoltaic cell, photons are absorbed and converted to electrical energy (light reaction). This leads to electric currents that have to be used immediately. Pursuing the long-term goal of direct fuel production from solar energy requires mimicking the other part of photosynthesis, conversion of CO_2 (dark reaction).

However, activating CO_2 and, more importantly, converting it to fuels is notoriously difficult due to the high stability of the CO_2 molecule, which imposes significant energy demands and requires high-temperature/pressure conditions and/or active reductants, such as hydrogen.[4−6] Alternatively, solid-state catalysts are needed. The vast majority of the autotrophs in nature fixate the inorganic carbon atom from CO_2 to produce sugars, during the dark reaction of photosynthesis, with an enzyme as catalyst: the Ribulose-1,5-bisphosphate carboxylase/oxygenase (RuBisCO, Figure 1a). This macroprotein is the most abundant protein in the biosphere. The active center of the RuBisCO is a Mg^{2+} ion surrounded by amino acid residues whose functions are to anchor the ribulose and provide the CO_2 as a cofactor bound to a lysil residue in the surroundings

Received: March 19, 2019
Accepted: May 22, 2019
Published: June 5, 2019

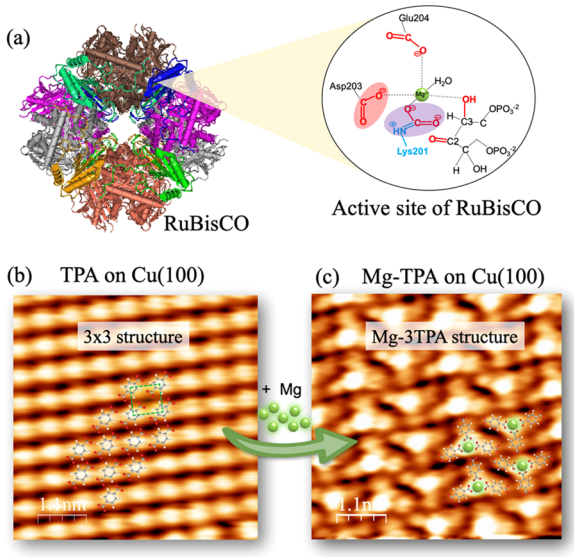

Figure 1. (a) Model of the enzyme RuBisCO and its active center.[40] (b) Scanning tunneling microscopy (STM) image of a typical terephthalic acid (TPA) network on Cu(100) at room temperature (RT). The inset shows the structural model of the fully deprotonated molecules arranged in a typical 3 × 3 configuration (V_{bias} = 1.122 V; i = 70 pA). (c) An STM image showing the structure formed by the co-deposition of TPA molecules and Mg atoms (V_{bias} = 0.821 V; i = 50 pA). The TPA molecules are characterized by the circular motifs whereas Mg, represented in the model by green circles, appears as circular protrusions between three TPA molecules. NB: the apparent height (brightness) of the Mg atoms depends on the tip conditions (see Figure S2).

of the Mg^{2+} (Figure 1a).[7] At lower levels of CO_2, O_2 molecules compete with CO_2. This competition consumes extra energy and, eventually, liberates CO_2. Thus, the enzyme is considered inefficient and motivates scientists to investigate ways to improve the enzymatic function of RuBisCO.

Metal−organic networks (MONs) are structures that resemble well the basic configuration of metalloenzymes.[8] They consist of metal nodes bound to organic bridging ligands that self-assemble on a metal substrate. These nanoarchitectures hold great potential in heterocatalysis due to the tunability of their metal centers,[9−11] organic linker, pore size,[12,13] and physical/chemical properties.[14−18] Even though many MONs were reported, the study of their catalytic properties with respect to gas adsorption is still in its infancy. Nevertheless, we consider that there is a critical mass of knowledge to attempt the inversion of the structure−function relationship. Our approach is then to apply the nanoarchitectonic principles learnt in the past two decades to start building structures that could resemble the architecture of the active site of known enzymes.[8,19] This approach promises to provide a playground where an atomistic insight into the relevant processes can be achieved, and, ultimately, it will allow us to create new bioinspired catalysts that could work at room temperature (RT). Moreover, the high level of control of the coordination environment allows us to evaluate separately the contribution of each functional group to the reactivity of the center.

Molecules with carboxylic functional groups (R-COOH) can work as excellent building blocks in the design of molecular nanostructures.[20] One characteristic is the deprotonation of COOH into a carboxylate group (COO^-) on solid surfaces at RT, which confers them the ability to form robust metal−organic networks with co-deposited transition[17,18,21−24] as well as alkali metal atoms.[25−28] Terephthalic acid (1,4-benzenedicarboxylic acid, TPA) is a model molecule that easily deprotonates on Cu surfaces at RT and eventually forms metal−organic networks with co-deposited adatoms.[17] A second characteristic is in regard to the oxygen atoms from its COO^- anions acting in the networks as electron acceptors,[29] which allow the control of the redox potential in the metal centers.[17,30] This particular feature encourages the use of metal−organic networks for O_2 dissociation,[8,30,31] aimed to resemble the catalytic function of enzymes specialized in O_2 reduction.[32,33]

The adsorption of CO_2 was recently explored on 2D metal−organic networks. One of the few examples involves the use of metal−organic chains of 1,4-phenylene diisocyanide molecules bound to Au adatoms on Au(111), to promote CO_2 capture at 77 K.[34,35] Moreover, networks formed by molecules with carboxylate groups bound to Fe centers have shown adsorption of CO_2 at 100 K.[36] Nevertheless, so far, no CO_2-driven phase transition has been reported at RT for any 2D metal−organic array.

Herein, inspired by the structure of the active site in the RuBisCO enzyme, we present a method to replicate the carboxylate environment around a Mg^{2+} ion. For this purpose, we designed an ionic network with Mg^{2+} as active centers by the self-assembly of TPA molecules with Mg atoms deposited on Cu(100) at RT. Finally, in the attempt to test the catalytic function of these bioinspired complexes, high partial pressures of CO_2 and O_2 are exposed on the system at RT. The stability and chemical changes in the network related to gas adsorption are studied by complementary techniques such as scanning tunneling microscopy (STM), high-resolution X-ray photoelectron spectroscopy (HR-XPS), and first principles density functional theory (DFT) calculations.

RESULTS AND DISCUSSION

Formation of Mg-TPA Networks on Cu(100). The main goal of this work is to mimic the catalytic function of the active site of the RuBisCO enzyme through the fabrication of 2D ionic networks with Mg^{2+} centers. Surface science studies have demonstrated that the catalytic activity of metal particles is boosted when they are reduced to single atoms,[37] as the coordination number decreases. Furthermore, organic molecules can coordinate adatoms from a metal surface, controlling the chemical environment around single atoms and their distribution, leaving apical orbitals ready to react with new species. This characteristic makes them good candidates to study their potential in heterogeneous catalysis. The first step in the strategy toward the formation of ionic networks with Mg adatoms consists in the formation of a self-assembled layer of the organic linkers. TPA molecules (coverage = 0.4 ML) were deposited on an atomically clean Cu(100) surface at RT. Earlier studies have reported that TPA molecules deprotonate and self-assemble on a Cu surface at RT.[38,39] Indeed, the typical STM image of this system (Figure 1b) shows a homomolecular patch of TPA forming a 3 × 3 phase structure (with respect to the underlying Cu surface) related to the self-assembly of fully deprotonated molecules.[38,39]

The second step consists in the co-deposition of sub-ML coverages of Mg atoms and TPA molecules on an atomically clean Cu(100) surface at RT (Figure 1c). The deposition process was finalized with postannealing at 353 K for 5 min to

DOI: 10.1021/acsomega.9b00762
ACS Omega 2019, 4, 9850−9859

favor the diffusion of the species on the surface. STM images (Figures 1c and S1) reveal the formation of a new structure incorporating single Mg atoms coordinated to three TPA molecules. Larger area images also show the presence of larger Mg clusters (bright circular protrusions) surrounded by TPA molecules (Figure S1-a). As we shall see, the presence of Mg clusters also agrees with XPS analysis in the Mg 2p region. Figure 1c shows that the molecules in the ordered islands get grouped in consecutive trigonal-planar arrangements, suggesting an electrostatic coordination to Mg^{2+}. The model superposed (obtained by DFT calculations) presents a structure based on a Mg^{2+} ion, represented as a green solid circle, coordinated by three TPA molecules through their carboxylate moieties. Two types of Mg−carboxylate coordination are present: one TPA with a bidentate carboxylate coupling to Mg, and two TPA carboxylates interacting via a monodentate coordination with Mg. From now on, this structure will be referred as Mg-3TPA. To the best of our knowledge, this is the first 2D metal−organic architecture that incorporates an alkaline earth metal atom (group 2) as a metal center.

A more precise configuration of the Mg-3TPA structure is described by DFT calculations. The calculations were performed using the Vienna ab initio simulation package (VASP),[41,42] including van der Waals (vdW) interaction within the vdW-dF scheme. Due to the large unit cell and the consequential computational overcharge, one monolayer of the Cu(100) surface with Cu atoms in fixed positions was included in the calculations, whereas the rest of the atoms forming the organic overlayer were allowed to relax until forces were smaller than 0.05 eV/Å. Tests including two substrate layers indicate a negligible (no more than a 2%) change in the vertical distances as compared with the calculations with a monolayer of the Cu substrate (see Figure S3 and Table S1). As a result, a relaxed Mg-3TPA ionic network was obtained on top of a Cu(100) layer. A Bader charge analysis[43,44] revealed the ionic character of Mg and O atoms due to the rearrangement of charge in the system. As seen in Figure 2a, for modeling the surface, a (10 × 5) unit cell was considered and the overlayer consists of two Mg atoms that lay at almost bridge positions on top of the surface, each of them coordinated with four O atoms from three different TPA molecules, i.e., six TPA molecules in total. The vertical distances from the atoms of the overlayer to the Cu surface vary from 1.96 Å the closest to 3.40 Å the largest. The two TPA units that are aligned with the [100] crystallographic direction get tilted around 7° and are anchored to the surface by the non-coordinated COO^- group, whereas the other two diagonal TPA units adopt an arched conformation. In agreement with the crystallographic database for the average bond distance in Mg−carboxylate networks,[45] the O−Mg distances for the monodentate and bidentate coordination are 2.03 and 2.20 Å, respectively. In addition, each TPA molecule forms H bonds (O···H−C) between two of their uncoordinated carboxylate moieties and the aromatic rings from adjacent molecules. To visualize the flux of charge due to the formation of the metal−organic compound, the electronic charge density difference is depicted in Figure 2b. The remarkable charge depletion (red) on the Mg positions and the charge accumulation (blue) in the O atoms that interact with the Mg adatom observed in Figure 2b represent a fingerprint of the ionic character of the complex formed. To confirm the reliability of the model, the Tersoff−Hamann approach[46,47]

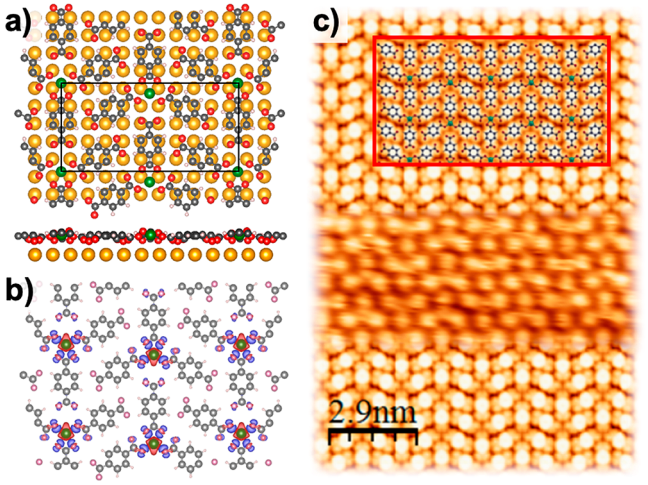

Figure 2. (a) Top and side views of the relaxed configuration of the ionic network on top of a Cu(100) layer calculated by means of DFT. The preferential geometry is based on Mg^{2+} ion coordinating three TPA molecules. The unit cell consists of two Mg^{2+} ions; each cation coordinates four carboxylate oxygens from three different TPA molecules. (b) Electronic density difference of the optimized structure showing the accumulation (blue) and depletion (red) of charge. Contour: 0.005 e^-. (c) Combined simulated STM image (top and bottom) of the system using the Tersoff−Hamann Approach with a bias voltage of −2 V and an experimental STM image (center).

was used to simulate STM images of a typical Mg-3TPA network (Figure 2c). The simulation was based on the integration of spatially resolved density of states in energy, from a certain applied bias potential (−2.0 eV) to the Fermi level. This simulation reproduced the zigzagging inversely ordered trigonal-planar arrangements seen in the experimental STM images of the Mg-3TPA network (see the combined image at the center of Figure 2c).

The chemical identity of TPA (Figure 3a) and Mg-3TPA (Figure 3b) networks on Cu(100) was confirmed by HR-XPS spectra. The XPS spectrum in the C 1s region of the reference system shows the typical profile of a homomolecular network containing fully deprotonated TPA molecules: an intense peak at 284.6 eV is attributed to the carbon atoms from the phenyl ring (6C), and a small peak at 287.6 eV, characteristic of carboxylate groups ($-COO^-$).[38] The dotted peak at 285.1 eV could be related to the different chemical environment around the aromatic carbons.[38] The 3 × 3 structure is also confirmed by the analysis of the XPS spectrum in the O 1s region, which contains a single peak at 531.3 eV attributed to carboxylate oxygens ($-COO^-$).

The shifts of the peaks in every spectrum in Figure 3b suggest an interaction between the co-deposited TPA molecules and Mg adatoms. On the one hand, the main peaks of the C 1s and O 1s binding energy regions in the network formed by the co-deposition of TPA molecules and Mg adatoms on Cu(100) (Figure 3b) are shifted toward higher binding energies, compared to those obtained for the TPA homomolecular network. Similar core level shifts were already reported as related to TPA molecules acquiring a protonated character on Cu(100).[38] However, TPA molecules are fully deprotonated under the present deposition conditions. Therefore, the protonated character of the negatively charged COO^- groups would be endowed by the Mg^{2+} cations, thus evidencing the formation of ionic networks. The detailed analysis in the C 1s region reveals a small peak at higher

DOI: 10.1021/acsomega.9b00762
ACS Omega 2019, 4, 9850−9859

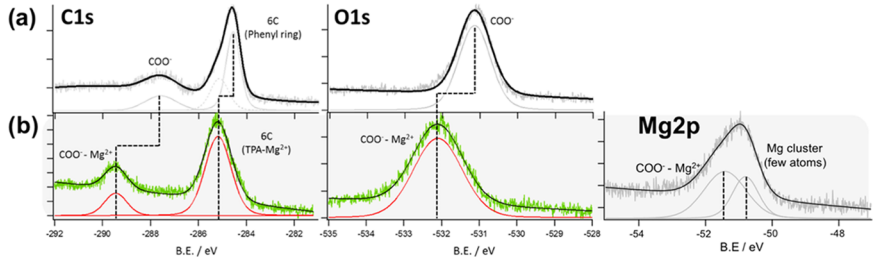

Figure 3. (a) HR-XPS spectra in the C 1s and O 1s binding energy regions of the homomolecular 3 × 3 phase of fully deprotonated TPA species on Cu(100). (b) HR-XPS spectra for a typical ionic network prepared by the co-deposition of TPA molecules and Mg atoms on Cu(100). The core level shifts in the C 1s and O 1s regions evidence the electrostatic interaction between Mg^{2+} and TPA species.

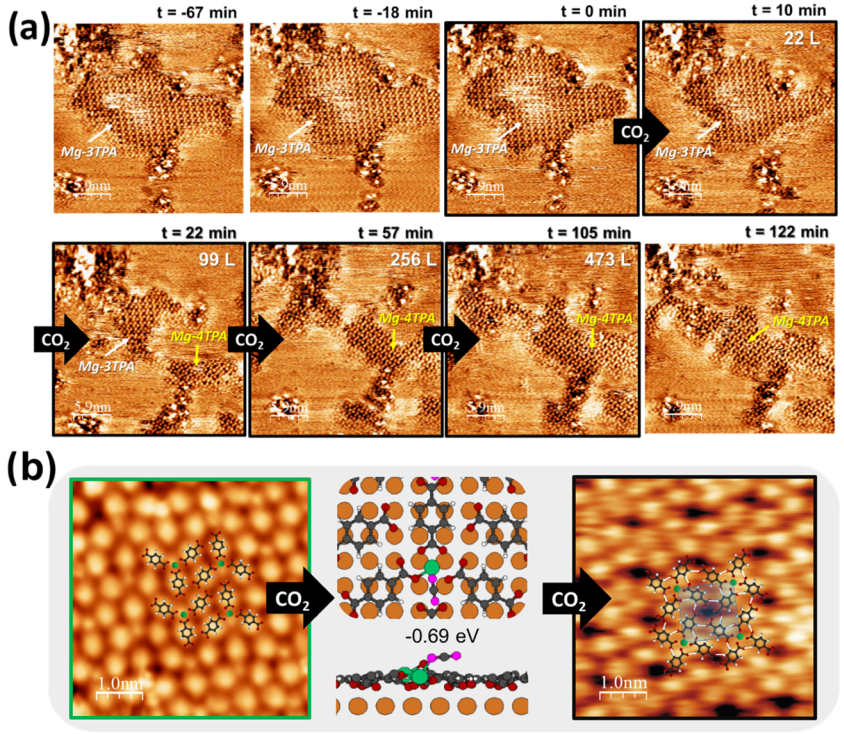

Figure 4. (a) Snapshots taken from a time-lapsed sequence of STM images for a Mg-3TPA ionic network on Cu(100) before, during (images with a black border), and after being exposed to CO_2. An irreversible structural change is observed: the Mg-3TPA network evolves to a Mg-4TPA structure (V_{bias} = −1.057 V; i = 73 pA). (b) Sketch of the CO_2−mediated transition from Mg-3TPA to Mg-4TPA. The middle panel shows a top and a side view of the Mg-3TPA model used to evaluate the local CO_2 adsorption. DFT calculations show that the intermediate between one structure and the other is based on the adsorption of a linear CO_2 molecule on the reactive Mg^{2+} center.

binding energies (289.4 eV), attributed to the electrostatic interaction between the COO^- group and the Mg^{2+} cations and an intense single peak at 285.2 eV, attributed to the 6C ring of the fully deprotonated TPA species interacting with Mg^{2+}. The remarkable core level shift to higher binding energies is associated to the charge migration from the C atoms toward the oxygen atoms in COO^-.[25] In addition, the O 1s line shape shows a dominant peak at 532.1 eV, related to a relative less negatively charged COO^- group due to the low electronic density around the core electrons during the electrostatic COO^-−Mg^{2+} interaction.[25] On the other hand, at lower energies, the Mg 2p binding energy region shows a broad peak that can be split in two components: one feature at 50.8 eV that reveals the presence of small Mg clusters on the surface and a second peak at 51.4 eV in the region corresponding to the ionic form of Mg (Mg^{2+}).[48−51] These two peaks suggest that TPA molecules sequestrate Mg atoms from clusters to eventually form ionic networks with Mg^{2+} cations. This mechanism may occur in a similar way as seen in ionic networks formed with alkali compounds.[52]

So far, we have described the formation of a 2D structure (Mg-3TPA) after the deposition of TPA molecules and Mg adatoms on Cu(100). This structure is stabilized by the ionic interactions between the carboxylate groups from TPA and the Mg^{2+} centers and resembles the carboxylate environment of the Mg^{2+} ion present in the active site of the RuBisCO enzyme. Next, we explore the catalytic properties of these ionic networks for gas adsorption.

Reactivity of 3 × 3 TPA and Mg-3TPA Ionic Networks with CO_2 and O_2. To study the reactivity of these assemblies, the 3 × 3 TPA and the Mg-3TPA adsorbed on Cu(100) structures were exposed to 470 L of CO_2 or 450 L of O_2. In the case of the homomolecular TPA network, STM images did not reveal any structural change neither when exposed to CO_2 nor O_2, preserving the 3 × 3 structure intact after gas exposure (Figure S4). Thus, we conclude that the pure TPA network

DOI: 10.1021/acsomega.9b00762
ACS Omega 2019, 4, 9850−9859

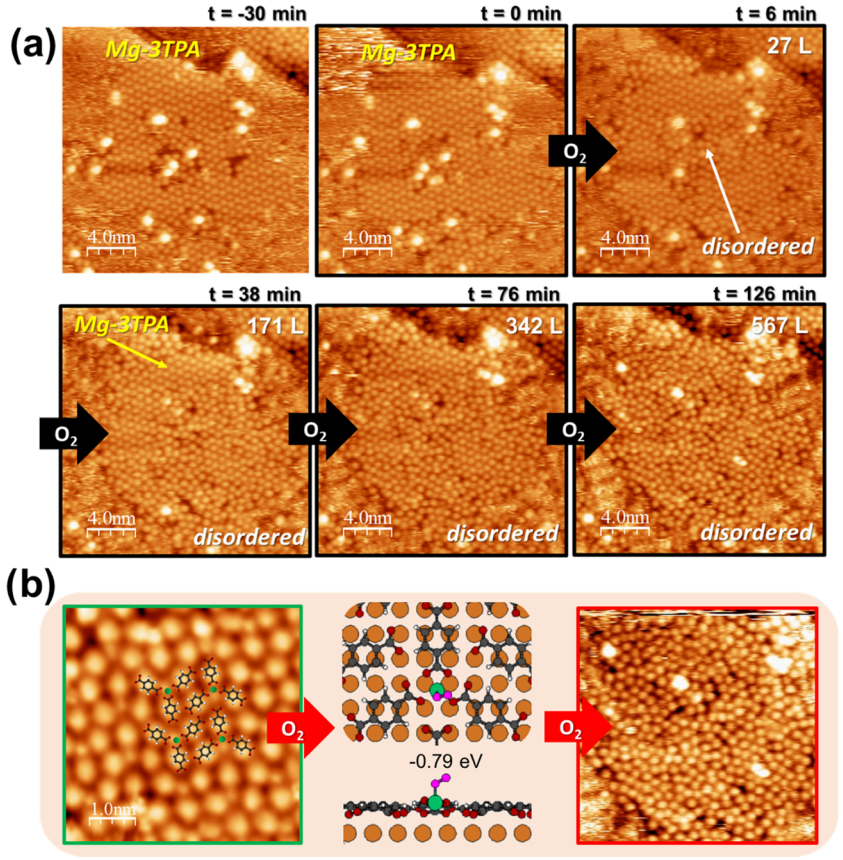

Figure 5. (a) Snapshots from a time-lapsed sequence of STM images for a TPA-Mg ionic network on Cu(100) taken before and during (images with a black border) O_2 exposure, where the Mg-3TPA evolves to a disordered molecular phase (V_{bias} = 1.189 V; i = 74 pA). (b) The interaction of O_2 induces the transition from Mg-3TPA to a disordered phase. The middle panel shows the intermediate structure of the local adsorption of O_2 obtained by DFT calculations.

does not interact either with CO_2 or with O_2. In fact, the molecular network passivates and protects the Cu surface for oxidation, as oxygen rows are only observed to grow in the bare Cu regions. To further verify the lack of chemical changes that could be undetectable by STM, HR-XPS experiments were also done. As shown in Figure S5, CO_2 is not absorbed in bare Cu regions at RT, as it cannot be detected in the C 1s and O 1s regions. Moreover, the 6C and COO^- signals in the C 1s region did not show any variation compared with the sample before gas exposure (Figure S5), confirming that CO_2 is not adsorbed in the molecular phase. Conversely, the exposure to O_2 molecules generates a peak at 529.7 eV characteristic of O^{-2} species chemisorbed on bare Cu surfaces,[53] whereas the peak at 531.3 eV remains at the same energy, confirming that the COO^- groups do not react with O_2. These experiments confirm that the TPA molecular phase is unreactive under CO_2 or O_2 exposure and that O_2 rows grow in the bare Cu areas, as seen by STM (S4).

This control experiment is important as proof of the formation of a reactive metal−organic network for two main reasons. First, the use of the same conditions to deposit TPA on Cu(100) at RT guarantees the full deprotonation of the molecules because carboxylate oxygens bind and control the redox potential of the metallic centers, and second, the unreactive character of COO^- groups against CO_2 and O_2 is crucial to discard the possible role of these groups as active centers when they self-assemble with Mg adatoms.

A typical ionic network with a Mg-3TPA configuration was prepared using the standard preparation process stated above. Figure 4a shows a series of consecutive STM images taken on a specific area of the surface over different periods of time. As seen in the first three images, the pristine Mg-3TPA structure was tracked during a period of 67 min and no structural changes were observed. Thus, the Mg-3TPA network was found suitable to test its reactivity under these conditions. Afterward, the interaction with CO_2 was tracked during almost 2 h. The first image (marked with a black border, snapshot with t = 0 min) represents the moment when CO_2 is released on the system. After only exposing 22 L of CO_2 (10 min), the surface area of the network decreases, providing the first evidence of reactivity. Then, after 99 L of CO_2 exposure (22 min), noticeable structural changes appear, related to a significant decrease of the Mg-3TPA network domain at the expense of a new phase forming at the bottom right side of the snapshot. The new phase presents a different configuration and it turns predominant after 256 L of CO_2 (57 min). This square-shaped structure organizes the molecules in a new motif: one Mg adatom surrounded by four TPA molecules leading to the formation of pores. From here on, this structure will be referred as Mg-4TPA. This new square-symmetrical arrangement suggests one type of Mg−carboxylate coordination: monodentate couplings (O−Mg) of the Mg center with each TPA molecule.[17] In addition, each TPA molecule forms H bonds (O···H−C) between two of their uncoordinated carboxylate moieties and the aromatic rings from adjacent

DOI: 10.1021/acsomega.9b00762
ACS Omega 2019, 4, 9850−9859

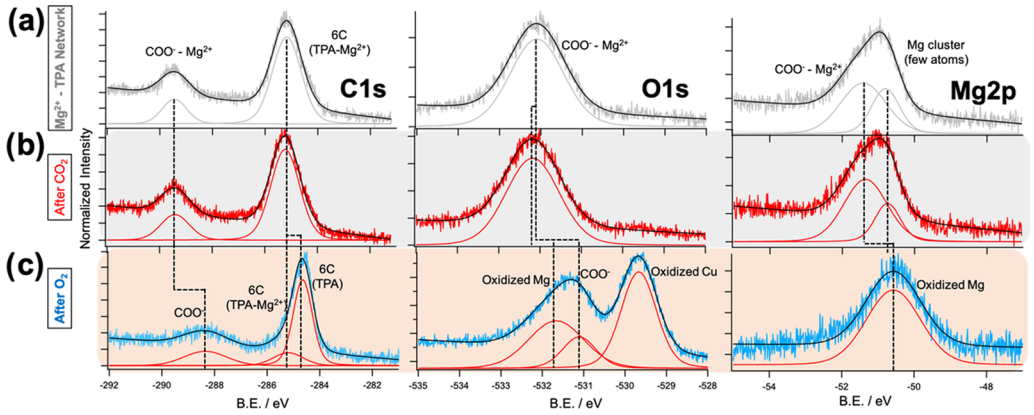

Figure 6. HR-XPS spectra showing the C 1s, O 1s, and Mg 2p binding energy regions for a typical Mg-3TPA network before (a) and after being exposed to 945 L of CO_2 (b) and 500 L of O_2 (c), respectively.

molecules (Figure 4b). The pores in the network are the result of the convergence of four uncoordinated carboxylate oxygens from four TPA molecules. After 473 L of CO_2 (105 min), the coverage of the predominant Mg-4TPA phase increases whereas the former Mg-3TPA structure vanishes completely. Finally, the CO_2 injection was stopped and the images were tracked during the next 17 min to observe whether or not the structure could reverse from a Mg-4TPA to Mg-3TPA configuration. The last snapshot at 122 min shows the stability of the Mg-4TPA structure with no signs of structural reversibility. Therefore, this experiment demonstrated that CO_2 catalyzed a phase transition: from a Mg-3TPA to Mg-4TPA configuration. This phase was also observed at high TPA/Mg ratios; in fact, Figure S6 shows pure TPA domains coexisting with the Mg-4TPA phase.

The structural changes observed by STM images encouraged the use of DFT calculations to study the local charge distribution in detail when CO_2 interacts with the ionic networks. Figure 4b shows that the presence of CO_2 distorts the local bonding in a Mg-3TPA structure. CO_2 adsorbs on the Mg^{2+} center in a linear configuration related to a weak chemisorption, with charge transfer weaker than that in a bent sp^2 configuration that is normally related to CO_2 chemisorption,[36] which requires the formation of the anion. In our DFT calculations, the adsorption energy of CO_2 on the Mg-3TPA network is −0.69 eV. This does not correspond to a full chemisorption, but this interaction seems to be strong enough to induce weakening of the bonds between Mg^{2+} and the carboxylate oxygens from TPA, disrupting the structure and inducing the binding of a fourth TPA to Mg^{2+} to form the Mg-4TPA structure (as seen after 22 min in Figure 4a). Many thorough studies have been related to the CO_2 adsorption on low-index Cu surfaces. On Cu(100), Cu(110), and Cu(111), CO_2 is physisorbed in a linear configuration at rather low temperature (and desorbed at 70−85 K) with adsorption energies in the ranges of 0.22−0.31 eV.[54,55] In a former paper, Campbell et. al.[56] indicate that the chemisorption of CO_2 on a clean Mg(0001) single crystal is dissociative, resulting in both surface oxide and carbonate species. Nevertheless, as we shall see from our XPS spectra, no signs of carbonates and magnesium oxides were detected during our experiments. Therefore, we conclude that the calculated adsorption energy of CO_2 on the Mg-3TPA network (more than twice the adsorption energy of CO_2 on bare Cu surfaces) is enough to produce an electronic rearrangement on the network, inducing a reconfiguration that triggers the formation of a new structure. However, no evidence of CO_2 dissociative adsorption is detected.

A second experiment was done to study the interaction of the ionic networks also with O_2 molecules. Again, consecutive STM images were taken on a defined area on the surface over different periods of time (Figure 5a). The first snapshot revealed the presence of the Mg-3TPA network and this ionic network did not show any structural changes during an interval of 30 min. The snapshots highlighted using a black border correspond to consecutive STM images taken during the O_2 exposition for a period of up to 2 h. The first structural change is observed after the exposure of 27 L of O_2 (6 min). The ionic network begins to disassemble from its center and this tendency continues while more O_2 is released in the system. Hence, after 171 L of O_2 (38 min) is exposed, most of the Mg-3TPA structure is disassembled. The disassembly is more evident after exposure of 342 L of O_2 (76 min), whereas the borders of the terraces also present strong signals of oxidation. Finally, a fully disordered structure is observed after exposure of 567 L of O_2 (126 min). Contrary to the case of CO_2 exposure, the structure never shows reorganization into an ordered configuration. These observations probe the direct interaction of O_2 with the system, which induces complete and irreversible disruption of the Mg-3TPA phase. Due to the disruption of the Mg-3TPA phase, an incipient formation of the 3 × 3 TPA phase is also observed together with the disordered phase (S7-a).

As described previously, CO_2 catalyzes phase transition from Mg-3TPA to Mg-4TPA. In contrast, the phase transition of Mg-3TPA to a disordered structure is rather specific to O_2. To study the local structure when O_2 interacts with the Mg-3TPA network, we performed DFT calculations showing the interactions of O_2 molecules on a Mg-3TPA network. The results showed that O_2 also binds nondissociatively through one of its oxygen atoms to the Mg^{2+} center of the ionic network (Figure 5b). The absorption energy of O_2 on top of a Mg^{2+} ion in the Mg-3TPA network was calculated to be −0.79 eV.

The interaction of a metal in an O_2-rich environment leads to the formation of a metal oxide that implies the dissociation of O_2. The Cu(001) surface is the most reactive among the low-index Cu surfaces to the adsorption and direct dissociation of O_2, as evidenced at various temperatures (even at 5 K).[57] On the other hand, the Mg(0001) surface also undergoes

DOI: 10.1021/acsomega.9b00762
ACS Omega 2019, 4, 9850−9859

oxidation at RT, leading to the formation of MgO thin films under exposure of O_2 doses.[51,58] Nevertheless, it was also demonstrated by first principles calculations that O_2 molecules can be incorporated into Mg adatoms by nondissociative adsorption to produce MgO_2 admolecules on a MgO(001) surface with point defects.[59] Thus, it is possible that after O_2 exposure, the uncovered Cu surface will undergo oxidation (by dissociation of O_2 molecules) and different oxidized Mg species will be formed in the network by dissociative and/or nondissociative interactions. Figure S7-b shows how O_2 molecules react with the Cu substrate (only when the surface is not fully covered by the Mg-3TPA network) and form the well-known oxygen rows on Cu(100).[60] Despite the fact that the DFT calculations are not conclusive (because the absorption energy difference between the physisorption of CO_2 and O_2 in the network is lower than expected), the calculated adsorption energy at the first step of the O_2 interaction is in good agreement with the trend observed experimentally. Therefore, the slightly higher adsorption energy obtained for O_2 seems to be enough to generate a reconfiguration of the charge around Mg^{2+} ions and to destabilize the COO^-—Mg^{2+} coordination leading to the dissociation of the metal—organic network.

The chemistry of CO_2 and O_2 interaction with the ionic networks was again contrasted using HR-XPS (Figure 6). As a reference, we included the Mg-3TPA ionic network spectra before gas exposure (Figure 6a). After 945 L of CO_2 exposure, XPS spectra do not show any significant change in the Mg 2p, C 1s, and O 1s binding energy regions (Figure 6b) compared to those in the Mg-3TPA network before exposure. As discussed above, CO_2 physisorbs on the Mg^{2+} center and it catalyzes a phase transition from a Mg-3TPA into Mg-4TPA structure. Therefore, the slight difference in the COO^-—Mg^{2+} coordination between both structures may produce changes in the chemical environment around Mg and O atoms. The Mg 2p region, shows an increment in the relative peak area at 51.4 eV (COO^-—Mg^{2+}) at the expense of the peak at 50.8 eV (Mg cluster with few atoms). This fact probes the action of CO_2 to enhance the segregation of the remaining small Mg clusters into Mg adatoms, which eventually coordinate with deprotonated TPA molecules to form larger patches of ionic network. Indeed, the segregation of the Mg clusters can be related to the joint action of CO_2 and deprotonated TPA molecules. It was shown above that fully deprotonated TPA species can segregate the clusters into single atoms of Mg, whose distribution on the surface is controlled by the COO^-—Mg^{2+} coordination. Thus, in contrast with ref 51, Mg atoms in the ionic network promote only a weak physisorption of CO_2, preventing the formation of $MgCO_3$.

Concerning the peaks related to C atoms from carboxylate (COO^-) and phenyl (6C) groups from the TPA molecules that form COO^-—Mg^{2+} coordination, they remain at 289.4 and 285.2 eV, respectively. Hence, the presence of physisorbed (if any) species of CO_2 is imperceptible. The presence of absorbed CO_2 is also elusive in the O 1s region (Figure 6b). The difficulty to identify the peaks related to CO_2 leads considering also the possibility that CO_2 may have left the system. Nevertheless, the consequences of the interaction of CO_2 on the system could be detected in the O 1s region where the peak at 532.2 eV (Mg^{2+}—COO^-) is slightly shifted by about 0.1 eV to higher binding energies. This shift could be related to the different coordination environment of the COO^- oxygens present in the recently formed Mg-4TPA configuration.

Summing up, even though CO_2 species cannot be observed within the time resolution of our XPS measurements, STM images and DFT calculations showed that the interaction of CO_2 is strong enough to reorganize the charge around Mg^{2+}, hence triggering a transition from Mg-3TPA to Mg-4TPA coordination. Thus, the ensemble of the results obtained by STM, DFT, and XPS suggests that CO_2 interacts with the system through temporary physisorption on Mg^{2+}.

The chemistry of O_2 adsorption in the ionic networks was also studied by HR-XPS. Figure 6c shows the Mg 2p, C 1s, and O 1s binding energy region of a Mg-3TPA network after 500 L of O_2 exposure. At first sight, it can be observed that the main peaks are shifted to lower binding energies compared with the Mg-3TPA network before O_2 exposure. The O 1s binding energy region shows an intense peak at lower binding energy (529.7 eV) related to the presence of oxidized Cu, as a consequence of the reactivity of O_2 with the bare Cu(100) areas, as confirmed also by the oxygen rows present in the STM image in Figure S7-b. However, the reactivity of O_2 with the ionic network is evidenced by the broader peak arising at a higher binding energy, whose deconvolution reveals two peaks at 531.1 and 531.6 eV. As studied by STM and DFT above, O_2 quenches the charge in the Mg^{2+} center and consequently disrupts the COO^-—Mg^{2+} interactions. In fact, the peak at 531.1 eV is characteristic of the COO^- group of deprotonated TPA molecules (see Figures SI and S2)[38] and confirms the disassembling of the TPA molecules from the ionic network. Accordingly, the peak at higher binding energy resembles the peak characteristic of the oxidized Mg species.[58]

The disassembling of the TPA molecules from the network is also confirmed in the C 1s region. The prominent peak at lower binding energies splits into two peaks: 284.6 and 285.2 eV, respectively. The peak at 284.6 eV is attributed to C6-ring carbons in fully deprotonated TPA molecules.[38] This peak presents a higher relative area compared with the smaller peak at 285.2 eV characteristic of the ionic networks, whose presence evidences the remaining small areas with the COO^-—Mg^{2+} coordination. Hence, the broad peak at higher binding energies at 288.4 eV is attributed to the wide range of contributions between the COO^- groups from the free molecules surrounded in a disordered fashion. Finally, the Mg 2p region, shows a broad peak at 50.6 eV attributed to Mg-oxidized species. Its shift to a lower binding energy would result from the effect of CuO on the substrate,[61] in a similar way as seen with larger Mg clusters exposed to O_2. These results demonstrated that the O_2 interaction induces the quenching of the charge without a complete breakdown of the COO^-—Mg^{2+} coordination. This implies that TPA molecules remain in a disordered configuration but they do not completely segregate to form a homomolecular network (in agreement with STM images, Figure 5a).

CONCLUSIONS

Inspired by the structure of the active site of RuBisCO, we have presented a method to synthesize a system based on a Mg^{2+} center stabilized by a carboxylate environment. Similar to the RuBisCO enzyme, the catalytic activity of the system was tested under high relative pressures of CO_2 and O_2 at RT. The Mg^{2+} centers were provided by the evaporation of Mg atoms on the surface. The full deprotonation of TPA molecules on Cu(100) at RT has been found suitable to provide the

DOI: 10.1021/acsomega.9b00762
ACS Omega 2019, 4, 9850−9859

carboxylate environment around the center of Mg^{2+}. The co-deposition of TPA molecules with Mg atoms on Cu(100) at RT resulted in the formation of a 2D ionic network. The structure was stabilized by the electrostatic interaction between Mg^{2+} and TPA species. The unit cell is formed by a single Mg^{2+} cation surrounded by three deprotonated TPA molecules (Mg-3TPA). The ionic networks have shown structural evidences of gas adsorption upon exposure to relative high-pressure doses of CO_2 or O_2. Both CO_2 and O_2 were found to interact with the Mg^{+2} center. The CO_2 molecules adsorb temporarily on Mg^{2+}, producing a charge imbalance that induced a phase transition into a different configuration (Mg-4TPA), whereas O_2 adsorbs on the Mg^{2+} center, giving rise to a distortion in the metal−organic bonds that eventually leads to the collapse of the structure. In both cases, the observed phase transitions showed that the ionic networks favor gas adsorption at RT. The 2D ionic network presented herein shows the potential of metal−organic coordination on surfaces to mimic enzymes active sites and track structural changes in situ under gas exposure by scanning probe microscopy, providing insight on the surface reactivity of coordinated metal centers and holding promise for the design of heterogeneous catalysts tailored down to the atomic level.

EXPERIMENTAL SECTION

STM experiments were performed in a homemade scanning tunneling microscope operated under ultra-high vacuum (UHV) conditions and repeated in the Omicron STM available at the synchrotron. This is an important experimental check to make sure that the networks we measured with XPS are the same measured by STM. The XPS data were acquired in the X-Ray beamline PEARL synchrotron facilities at the Paul Scherrer Institute (PSI), Switzerland. The data for the Mg 2p, C 1s, and O 1s were acquired with a beam energy of 160, 370, and 650 eV, respectively. The pass energy of the analyzer was set to 20 eV. The spectra were referenced using the Au $4f_{7/2}$ line at 84.1 eV. All experiments were carried out under UHV ($\sim 3 \times 10^{-10}$ mbar) at RT.

Substrate Preparation. A Cu(001) single crystal (Mateck) is used as a substrate. The cleaning process was performed in the UHV chamber with a base pressure of 5.0×10^{-10} mbar. The surface was cleaned by consecutive cycles of Ar^+ sputtering (0.5 keV) and annealing at temperatures up to 810 K, followed by a slow and gradual cooling down of the crystal to 313 K before starting with the next cleaning cycle.

Sample Preparation. 1,4-Benzenedicarboxylic acid (TPA) molecules (Fluka) were deposited by thermal evaporation from a quartz crucible by heating it up to 448 K. During molecular deposition, the pressure in the chamber was kept below 2.0×10^{-9} mbar while the temperature of the substrates was kept at RT. Before deposition, the molecules were fully degassed.

COMPUTATIONAL DETAILS

DFT calculations were carried out using the 5.4.4 version of VASP.[42,62,63] For the description of electron−ion interactions the projector-augmented wave method was employed, whereas the Perdew, Burke, and Ernzerhof functional was used to describe exchange and correlation within the generalized gradient approximation[64] and optB88-vdW functional to describe the nonlocal van der Waals interaction.[65]

The periodic slab models include a Cu layer, the two nonequivalent Mg-3(4)TPA units, and 15 Å of vacuum. A $2 \times 2 \times 1$ Monkhorst-Pack mesh is used to describe the unit cell, and the plane-wave energy cutoff was 400 eV in all cases. To perform the relaxation of the Mg−organic network on top of the Cu (001) surface, all atoms of the network were relaxed until the forces were less than 0.05 eV/Å and a convergence criterion of 10^{-4} eV was used for energy. However, when the small reactants were included, only the latter and the corresponding Mg center and the surrounding carboxylate groups were allowed to relax.

VESTA software[66] was used to represent the geometrical and electronically induced density models with output data of the previous calculations. The STM simulation of the adsorbed Mg-TPA on Cu(100) substrate in the Tersoff−Hamann approach was done with WSxM software.[67]

ASSOCIATED CONTENT

Supporting Information

The Supporting Information is available free of charge on the ACS Publications website at DOI: 10.1021/acsomega.9b00762.

Additional STM images showing the structure of the metal−organic network, STM images and XPS spectra showing that TPA networks remain intact after gas exposure and partial oxidation of the bare Cu surface, and additional computational details (PDF)

AUTHOR INFORMATION

Corresponding Authors

*E-mail: fernando.cometto@epfl.ch (F.P.C.).
*E-mail: magali.lingenfelder@epfl.ch (M.L.).

ORCID

Fernando P. Cometto: 0000-0002-0825-2312
Magalí Lingenfelder: 0000-0003-1362-8879

Notes

The authors declare no competing financial interest.

ACKNOWLEDGMENTS

We acknowledge the support of Dr. G. Ruano during the first phase of this project and Dr. M. Muntwiler and Dr. J. Zhang during our beamtimes at PEARL, PSI, Switzerland. A.S. and A.A. acknowledge support from the Spanish Ministerio de Ciencia e Innovación (Grant No. FIS2016-75862-P).

REFERENCES

(1) Krause, G. H.; Weis, E. Chlorophyll Fluorescence and Photosynthesis: The Basics. *Annu. Rev. Plant Physiol. Plant Mol. Biol.* **1991**, *42*, 313−349.

(2) Sharma, V. K.; Colangelo, A.; Spagna, G. Photovoltaic Technology: Basic Concepts, Sizing of a Stand Alone Photovoltaic System for Domestic Applications and Preliminary Economic Analysis. *Energy Convers. Manage.* **1995**, *36*, 161−174.

(3) Singh, G. K. Solar Power Generation by PV (Photovoltaic) Technology: A Review. *Energy* **2013**, *53*, 1−13.

(4) Ma, J.; Sun, N.; Zhang, X.; Zhao, N.; Xiao, F.; Wei, W.; Sun, Y. A Short Review of Catalysis for CO2 Conversion. *Catal. Today* **2009**, *148*, 221−231.

(5) Baiker, A. Utilization of Carbon Dioxide in Heterogeneous Catalytic Synthesis. *Appl. Organomet. Chem.* **2000**, *14*, 751−762.

(6) Chueh, W. C.; Falter, C.; Abbott, M.; Scipio, D.; Furler, P.; Haile, S. M.; Steinfeld, A. High-Flux Solar-Driven Thermochemical Dissociation of CO_2 and H_2O Using Nonstoichiometric Ceria. *Science* **2010**, *330*, 1797−1801.

DOI: 10.1021/acsomega.9b00762
ACS Omega 2019, 4, 9850−9859

(7) Andrews, T. J. The Bait in the Rubisco Mousetrap. *Nat. Struct. Mol. Biol.* **1996**, *3*, 3−7.
(8) Gutzler, R.; Stepanow, S.; Grumelli, D.; Lingenfelder, M.; Kern, K. Mimicking Enzymatic Active Sites on Surfaces for Energy Conversion Chemistry. *Acc. Chem. Res.* **2015**, *48*, 2132−2139.
(9) Pawin, G.; Wong, K. L.; Kim, D.; Sun, D.; Bartels, L.; Hong, S.; Rahman, T. S.; Carp, R.; Marsella, M. A Surface Coordination Network Based on Substrate-Derived Metal Adatoms with Local Charge Excess. *Angew. Chem., Int. Ed.* **2008**, *47*, 8442−8445.
(10) Lin, N.; Dmitriev, A.; Weckesser, J.; Barth, J. V.; Kern, K. Real-Time Single-Molecule Imaging of the Formation and Dynamics of Coordination Compounds. *Angew. Chem., Int. Ed.* **2002**, *41*, 4779−4783.
(11) Jensen, S.; Baddeley, C. J. Formation of PTCDI-Based Metal Organic Structures on a Au(111) Surface Modified by 2-D Ni Clusters. *J. Phys. Chem. C* **2008**, *112*, 15439−15448.
(12) Schlickum, U.; Decker, R.; Klappenberger, F.; Zoppellaro, G.; Klyatskaya, S.; Ruben, M.; Silanes, I.; Arnau, A.; Kern, K.; Brune, H.; et al. Metal−Organic Honeycomb Nanomeshes with Tunable Cavity Size. *Nano Lett.* **2007**, *7*, 3813−3817.
(13) Kühne, D.; Klappenberger, F.; Decker, R.; Schlickum, U.; Brune, H.; Klyatskaya, S.; Ruben, M.; Barth, J. V. High-Quality 2D Metal−Organic Coordination Network Providing Giant Cavities within Mesoscale Domains. *J. Am. Chem. Soc.* **2009**, *131*, 3881−3883.
(14) Barth, J. V.; Costantini, G.; Kern, K. Engineering Atomic and Molecular Nanostructures at Surfaces. *Nature* **2005**, *437*, 671−679.
(15) Stepanow, S.; Lin, N.; Barth, J. V. Modular Assembly of Low-Dimensional Coordination Architectures on Metal Surfaces. *J. Phys.: Condens. Matter* **2008**, *20*, No. 184002.
(16) Dmitriev, A.; Spillmann, H.; Lingenfelder, M.; Lin, N.; Barth, J. V.; Kern, K. Design of Extended Surface-Supported Chiral Metal-Organic Arrays Comprising Mononuclear Iron Centers. *Langmuir* **2004**, *20*, 4799−4801.
(17) Lingenfelder, M. A.; Spillmann, H.; Dmitriev, A.; Stepanow, S.; Lin, N.; Barth, J. V.; Kern, K. Towards Surface-Supported Supramolecular Architectures: Tailored Coordination Assembly of 1,4-Benzenedicarboxylate and Fe on Cu(100). *Chem. - Eur. J.* **2004**, *10*, 1913−1919.
(18) Barth, J. V. Molecular Architectonic on Metal Surfaces. *Annu. Rev. Phys. Chem.* **2007**, *58*, 375−407.
(19) Dong, L.; Gao, Z.; Lin, N. Self-Assembly of Metal−Organic Coordination Structures on Surfaces. *Prog. Surf. Sci.* **2016**, *91*, 101−135.
(20) Lingenfelder, M.; Fuhr, J. D.; Gayone, J. E.; Ascolani, H. Carboxylate Groups: Deprotonation of Carboxylic Acids and Formation of Coordination Networks. In *Reference Module in Chemistry, Molecular Sciences and Chemical Engineering*; 01/2017; ISBN: 9780124095472.
(21) Stepanow, S.; Lingenfelder, M.; Dmitriev, A.; Spillmann, H.; Delvigne, E.; Lin, N.; Deng, X.; Cai, C.; Barth, J. V.; Kern, K. Steering Molecular Organization and Host−Guest Interactions Using Two-Dimensional Nanoporous Coordination Systems. *Nat. Mater.* **2004**, *3*, 229−233.
(22) Wang, Y.; Lingenfelder, M.; Fabris, S.; Fratesi, G.; Ferrando, R.; Classen, T.; Kern, K.; Costantini, G. Programming Hierarchical Supramolecular Nanostructures by Molecular Design. *J. Phys. Chem. C* **2013**, *117*, 3440−3445.
(23) Ge, Y.; Adler, H.; Theertham, A.; Kesmodel, L. L.; Tait, S. L. Adsorption and Bonding of First Layer and Bilayer Terephthalic Acid on the Cu(100) Surface by High-Resolution Electron Energy Loss Spectroscopy. *Langmuir* **2010**, *26*, 16325−16329.
(24) Wang, Y.; Fabris, S.; White, T. W.; Pagliuca, F.; Moras, P.; Papagno, M.; Topwal, D.; Sheverdyaeva, P.; Carbone, C.; Lingenfelder, M.; et al. Varying Molecular Interactions by Coverage in Supramolecular Surface Chemistry. *Chem. Commun.* **2012**, *48*, 534−536.
(25) Stepanow, S.; Ohmann, R.; Leroy, F.; Lin, N.; Strunskus, T.; Wöll, C.; Kern, K. Rational Design of Two-Dimensional Nanoscale Networks by Electrostatic Interactions at Surfaces. *ACS Nano* **2010**, *4*, 1813−1820.
(26) Xu, W.; Tan, Q.; Yu, M.; Sun, Q.; Kong, H.; Lægsgaard, E.; Stensgaard, I.; Kjems, J.; Wang, J.; Wang, C.; et al. Atomic-Scale Structures and Interactions between the Guanine Quartet and Potassium. *Chem. Commun.* **2013**, *49*, 7210−7212.
(27) Wäckerlin, C.; Iacovita, C.; Chylarecka, D.; Fesser, P.; Jung, T. A.; Ballav, N. Assembly of 2D Ionic Layers by Reaction of Alkali Halides with the Organic Electrophile 7,7,8,8-Tetracyano-p-Quinodimethane (TCNQ). *Chem. Commun.* **2011**, *47*, 9146−9148.
(28) Skomski, D.; Abb, S.; Tait, S. L. Robust Surface Nano-Architecture by Alkali−Carboxylate Ionic Bonding. *J. Am. Chem. Soc.* **2012**, *134*, 14165−14171.
(29) Ruben, M.; Payer, D.; Landa, A.; Comisso, A.; Gattinoni, C.; Lin, N.; Collin, J.-P.; Sauvage, J.-P.; De Vita, A.; Kern, K. 2D Supramolecular Assemblies of Benzene-1,3,5-Triyl-Tribenzoic Acid: Temperature-Induced Phase Transformations and Hierarchical Organization with Macrocyclic Molecules. *J. Am. Chem. Soc.* **2006**, *128*, 15644−15651.
(30) Tait, S. L.; Wang, Y.; Costantini, G.; Lin, N.; Baraldi, A.; Esch, F.; Petaccia, L.; Lizzit, S.; Kern, K. Metal−Organic Coordination Interactions in Fe−Terephthalic Acid Networks on Cu(100). *J. Am. Chem. Soc.* **2008**, *130*, 2108−2113.
(31) Fabris, S.; Stepanow, S.; Lin, N.; Gambardella, P.; Dmitriev, A.; Honolka, J.; Baroni, S.; Kern, K. Oxygen Dissociation by Concerted Action of Di-Iron Centers in Metal−Organic Coordination Networks at Surfaces: Modeling Non-Heme Iron Enzymes. *Nano Lett.* **2011**, *11*, 5414−5420.
(32) Skomski, D.; Tempas, C. D.; Smith, K. A.; Tait, S. L. Redox-Active On-Surface Assembly of Metal−Organic Chains with Single-Site Pt(II). *J. Am. Chem. Soc.* **2014**, *136*, 9862−9865.
(33) Costas, M.; Mehn, M. P.; Jensen, M. P.; Que, L. Dioxygen Activation at Mononuclear Nonheme Iron Active Sites: Enzymes, Models, and Intermediates. *Chem. Rev.* **2004**, *104*, 939−986.
(34) Feng, M.; Sun, H.; Zhao, J.; Petek, H. Self-Catalyzed Carbon Dioxide Adsorption by Metal−Organic Chains on Gold Surfaces. *ACS Nano* **2014**, *8*, 8644−8652.
(35) Feng, M.; Petek, H.; Shi, Y.; Sun, H.; Zhao, J.; Calaza, F.; Sterrer, M.; Freund, H.-J. Cooperative Chemisorption-Induced Physisorption of CO2 Molecules by Metal−Organic Chains. *ACS Nano* **2015**, *9*, 12124−12136.
(36) Čechal, J.; Kley, C. S.; Pétuya, R.; Schramm, F.; Ruben, M.; Stepanow, S.; Arnau, A.; Kern, K. CO2 Binding and Induced Structural Collapse of a Surface-Supported Metal−Organic Network. *J. Phys. Chem. C* **2016**, *120*, 18622−18630.
(37) Yang, X.-F.; Wang, A.; Qiao, B.; Li, J.; Liu, J.; Zhang, T. Single-Atom Catalysts: A New Frontier in Heterogeneous Catalysis. *Acc. Chem. Res.* **2013**, *46*, 1740−1748.
(38) Stepanow, S.; Strunskus, T.; Lingenfelder, M.; Dmitriev, A.; Spillmann, H.; Lin, N.; Barth, J. V.; Wöll, Ch.; Kern, K. Deprotonation-Driven Phase Transformations in Terephthalic Acid Self-Assembly on Cu(100). *J. Phys. Chem. B* **2004**, *108*, 19392−19397.
(39) Fuhr, J. D.; Carrera, A.; Murillo-Quirós, N.; Cristina, L. J.; Cossaro, A.; Verdini, A.; Floreano, L.; Gayone, J. E.; Ascolani, H. Interplay between Hydrogen Bonding and Molecule−Substrate Interactions in the Case of Terephthalic Acid Molecules on Cu(001) Surfaces. *J. Phys. Chem. C* **2013**, *117*, 1287−1296.
(40) Taylor, T. C.; Andersson, I. The Structure of the Complex between Rubisco and Its Natural Substrate Ribulose 1,5-Bisphosphate. *J. Mol. Biol.* **1997**, *265*, 432−444.
(41) Kresse, G.; Hafner, J. Ab Initio. *Phys. Rev. B* **1993**, *47*, 558−561.
(42) Kresse, G.; Furthmüller, J. Efficient Iterative Schemes for Ab Initio Total-Energy Calculations Using a Plane-Wave Basis Set. *Phys. Rev. B* **1996**, *54*, 11169−11186.
(43) Bader, R. F. W. *Atoms in Molecules: A Quantum Theory*; 1st Paperback ed., Clarendon Press: Oxford England, 1994.

DOI: 10.1021/acsomega.9b00762
ACS Omega 2019, 4, 9850−9859

(44) Popelier, P. L. *Atoms in Molecules: An Introduction*, 1st ed.; Prentice-Hall: Harlow, 2000.
(45) Banerjee, D.; Parise, J. B. Recent Advances in S-Block Metal Carboxylate Networks. *Cryst. Growth Des.* **2011**, *11*, 4704−4720.
(46) Tersoff, J.; Hamann, D. R. Theory of the Scanning Tunneling Microscope. *Phys. Rev. B* **1985**, *31*, 805−813.
(47) Tersoff, J.; Hamann, D. R. Theory and Application for the Scanning Tunneling Microscope. *Phys. Rev. Lett.* **1983**, *50*, 1998−2001.
(48) Corneille, J. S.; He, J.-W.; Goodman, D. W. XPS Characterization of Ultra-Thin MgO Films on a Mo(100) Surface. *Surf. Sci.* **1994**, *306*, 269−278.
(49) Chen, C.; Splinter, S. J.; Do, T.; McIntyre, N. S. Measurement of Oxide Film Growth on Mg and Al Surfaces over Extended Periods Using XPS. *Surf. Sci.* **1997**, *382*, L652−L657.
(50) Splinter, S. J.; McIntyre, N. S.; Lennard, W. N.; Griffiths, K.; Palumbo, G. An AES and XPS Study of the Initial Oxidation of Polycrystalline Magnesium with Water Vapour at Room Temperature. *Surf. Sci.* **1993**, *292*, 130−144.
(51) Peng, X. D.; Barteau, M. A. Characterization of Oxide Layers on Mg(0001) and Comparison of H2O Adsorption on Surface and Bulk Oxides. *Surf. Sci.* **1990**, *233*, 283−292.
(52) Skomski, D.; Abb, S.; Tait, S. L. Robust Surface Nano-Architecture by Alkali-Carboxylate Ionic Bonding. *J. Am. Chem. Soc.* **2012**, *134*, 14165−14171.
(53) Copperthwaite, R. G.; Davies, P. R.; Morris, M. A.; Roberts, M. W.; Ryder, R. A. The Reactive Chemisorption of Carbon Dioxide at Magnesium and Copper Surfaces at Low Temperature. *Catal. Lett.* **1988**, *1*, 11−19.
(54) Ernst, K.-H.; Schlatterbeck, D.; Christmann, K. Adsorption of Carbon Dioxide on Cu(110) and on Hydrogen and Oxygen Covered Cu(110) Surfaces. *Phys. Chem. Chem. Phys.* **1999**, *1*, 4105−4112.
(55) Muttaqien, F.; Hamamoto, Y.; Hamada, I.; Inagaki, K.; Shiozawa, Y.; Mukai, K.; Koitaya, T.; Yoshimoto, S.; Yoshinobu, J.; Morikawa, Y. CO2 Adsorption on the Copper Surfaces: Van Der Waals Density Functional and TPD Studies. *J. Chem. Phys.* **2017**, *147*, No. 094702.
(56) Campbell, S.; Hollins, P.; McCash, E.; Roberts, M. W. Reaction of Carbon Dioxide with the Magnesium(0001) Surface. *J. Electron Spectrosc. Relat. Phenom.* **1986**, *39*, 145−153.
(57) Yagyu, K.; Liu, X.; Yoshimoto, Y.; Nakatsuji, K.; Komori, F. Dissociative Adsorption of Oxygen on Clean Cu(001) Surface. *J. Phys. Chem. C* **2009**, *113*, 5541−5546.
(58) Kurth, M.; Graat, P. C. J.; Mittemeijer, E. J. Determination of the Intrinsic Bulk and Surface Plasmon Intensity of XPS Spectra of Magnesium. *Appl. Surf. Sci.* **2003**, *220*, 60−78.
(59) Geneste, G.; Morillo, J.; Finocchi, F. Adsorption and Diffusion of Mg, O, and O2 on the MgO(001) Flat Surface. *J. Chem. Phys.* **2005**, *122*, No. 174707.
(60) Lahtonen, K.; Hirsimäki, M.; Lampimäki, M.; Valden, M. Oxygen Adsorption-Induced Nanostructures and Island Formation on Cu{100}: Bridging the Gap between the Formation of Surface Confined Oxygen Chemisorption Layer and Oxide Formation. *J. Chem. Phys.* **2008**, *129*, No. 124703.
(61) Isahak, W. N. R. W.; Hasan, S. Z.; Ramli, Z. A. C.; Ba-Abbad, M. M.; Yarmo, M. A. Enhanced Physical and Chemical Adsorption of Carbon Dioxide Using Bimetallic Copper−Magnesium Oxide/Carbon Nanocomposite. *Res. Chem. Intermed.* **2017**, *44*, 829−841.
(62) Kresse, G.; Hafner, J. Ab Initio Molecular Dynamics for Liquid Metals. *Phys. Rev. B* **1993**, *47*, 558−561.
(63) Kresse, G.; Furthmüller, J. Efficiency of Ab-Initio Total Energy Calculations for Metals and Semiconductors Using a Plane-Wave Basis Set. *Comput. Mater. Sci.* **1996**, *6*, 15−50.
(64) Perdew, J. P.; Burke, K.; Ernzerhof, M. Generalized Gradient Approximation Made Simple. *Phys. Rev. Lett.* **1996**, *77*, 3865−3868.
(65) Klimeš, J.; Bowler, D. R.; Michaelides, A. Van Der Waals Density Functionals Applied to Solids. *Phys. Rev. B* **2011**, *83*, No. 195131.
(66) Momma, K.; Izumi, F. VESTA 3 for Three-Dimensional Visualization of Crystal, Volumetric and Morphology Data. *J. Appl. Crystallogr.* **2011**, *44*, 1272−1276.
(67) Horcas, I.; Fernández, R.; Gómez-Rodríguez, J. M.; Colchero, J.; Gómez-Herrero, J.; Baro, A. M. WSXM: A Software for Scanning Probe Microscopy and a Tool for Nanotechnology. *Rev. Sci. Instrum.* **2007**, *78*, No. 013705.

DOI: 10.1021/acsomega.9b00762
ACS Omega 2019, 4, 9850−9859